Comparison of reversible and irreversible actuators for statically stable walking robots from the point of view of the energy consumption

J Roca[1], M Bobi[1], E Celaya[2], S Cardona[3]
[1]Universitat de Lleida – Departament d'Informàtica i Enginyeria Industrial
Jaume II, 69 – 25001 Lleida – Spain
[2]Institut de Robòtica i Informàtica Industrial
Llorens i Artigas, 4-6 – 08028 Barcelona – Spain
[3]Universitat Politècnica de Catalunya – Departament d'Enginyeria Mecànica
Diagonal, 647 – 08028 Barcelona – Spain
email: jroca@diei.udl.es, celaya@iri.upc.es, salvador.cardona@upc.edu

Abstract: **This paper presents the energetic analysis corresponding to different alternatives of driving system for joint actuation of a statically stable hexapod robot. Inertia of rotating parts in the actuator, and the friction between moving parts have an important influence on the energy consumption. Special attention is made to the influence of the reversibility or irreversibility of the transmission on the global energy balance.**

Leg mechanisms simulation has been carried out using a commercial CAD-CAE software in order to obtain joint actuator requirements during operation. Two operating modes are studied: walking on a horizontal ground and standing still. Friction and rotational inertia models are defined for each actuator component.

Finally, actuators models are used to simulate their operation in order to evaluate the transmitted power between actuator components. The main result is the estimated electrical energy consumption per cycle of each actuator alternative.

Keywords: **walking robot, actuator, energy consumption**

I. Introduction

Several are the causes responsible for the high power consumption of walking machines. Many actuators are necessary for the multiple degrees of freedom, leading to a high mass of the robot [1], and often the efficiency of the actuator components, motors and transmissions, are quite poor. In addition, most of the joints and actuators work at highly variable speed, which implies an important kinetic energy fluctuation that results in an increased energy loss due to friction [2].

This paper focuses on the study of a statically stable walking robot, which is more easily controllable and suitable for many applications than dynamically stable robots [3]. On the other hand, the energy consumption can be higher, because there is no mechanical energy storage during operation.

Many operating modes are possible in walking robots [4]. Some examples are: advancing at different speeds, walking on a flat or on an unstructured terrain, avoiding obstacles, or standing still while performing some tasks. In each case, the relative importance of the inertial and the frictional effects in the actuator are different. In particular, friction contributes to save energy when the robot stays still, but produces the contrary effect when moving. The selection of the actuator components should depend on the predominant operating modes of the robot. So, in order to make a correct choice, it is necessary to analyse the energy loses or savings caused by frictional and inertial effects in different operating modes.

Following sections present the whole simulation process, starting from actuator requirements definition. Later, different actuator alternatives are described focusing on their components features. At this point, friction and rotational inertia models formulation is presented for each alternative. Then, simulations are run and results of electrical energy consumption are obtained and analysed. Eventually, results are discussed in the conclusions section.

II. Actuator requirements in a 3 joint leg mechanism

Two operating modes have been analysed for this energy consumption study: walking on a horizontal ground and standing still.

A. Robot specifications and leg configuration

The main specifications of the statically stable, hexapod walking robot are shown in Table I. Robot size is decided in order to be able to operate in a human environment and the total mass is estimated including control hardware and batteries. Main dimensions can also be seen in Fig. 1. The same leg design is used for the six legs of the hexapod.

TABLE I

Specifications of the hexapod robot

Body length [mm]	600
Robot width [mm]	520
Femur length [mm]	180
Tibia length [mm]	340
Total robot mass [kg]	40

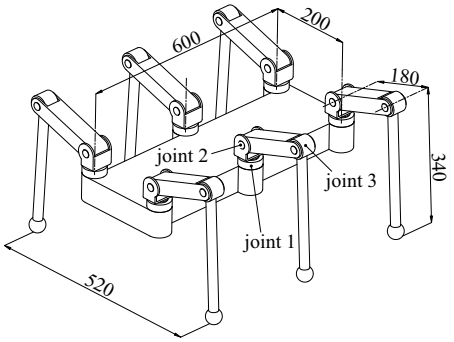

Fig. 1. Hexapod layout and the 3 joints of a leg.

B. *Actuators requirements during a standard walking cycle*

The walking operation considered in this study corresponds to a tripod gait and the robot advancing at constant speed on a flat and horizontal surface. Walking parameters are presented in Table II.

TABLE II

WALKING PARAMETERS FOR TRIPOD GAIT

Longitudinal foot stroke [mm]	240
Vertical foot stroke [mm]	75
Robot walking speed [m/min]	9,6
Gait period [s]	3

A commercial CAD-CAE software has been used to run simulations. In order to solve the redundancies of the contact forces between feet and ground, it is assumed that the tangential forces at the feet are the minimum ones which guarantee the desired robot motion. The results of the simulations are velocity and torque demands to ensure the desired trajectory of the foot. No friction is considered at the joints in this simulation, since all friction effects will be taken into account later, when the driving system is analysed.

Simulations results of the analysed gait for the middle-right leg are represented in Fig. 2 to 4. Support phase is from 0 to 1,5 s and transfer phase from 1,5 to 3 s.

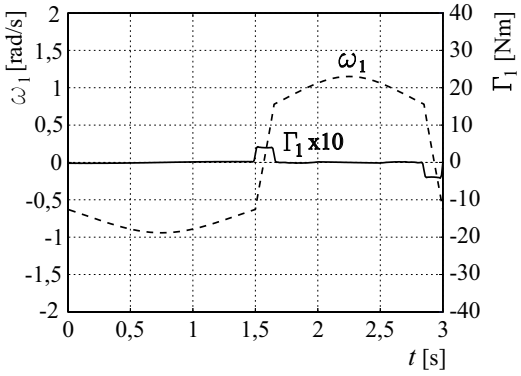

Fig. 2. Velocity and torque demand at joint 1 during a walking cycle.

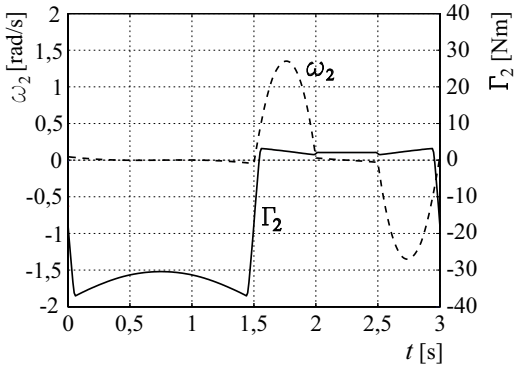

Fig. 3. Velocity and torque demand at joint 2 during a walking cycle.

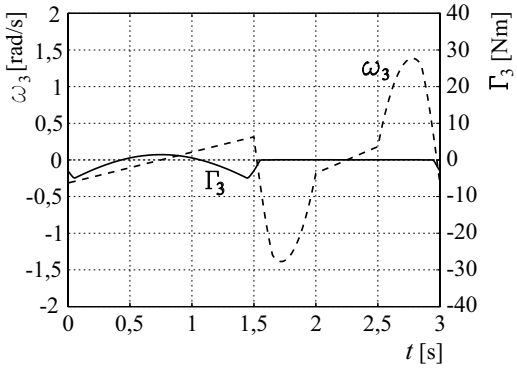

Fig. 4. Velocity and torque demand at joint 3 during a walking cycle.

C. *Actuators requirements when the robot is standing still*

The situation that has been analysed in this case corresponds to the robot supported on three legs, the minimum to guarantee the stability. The considered supporting legs are front and rear ones on the left side and middle-right leg on the right side, and the mechanism configuration of each leg is when the foot is at the middle of its longitudinal stroke.

At the middle-right leg, the vertical reaction between ground and foot is 192,6 N. Then torque demand at each joint of this leg, according to mechanism simulation, is shown in Table III.

TABLE III

TORQUE DEMAND AT EACH JOINT WHEN STANDING STILL

Joint	1	2	3
Γ_{out} [Nm]	0	-30,71	1,46

III. ACTUATOR ALTERNATIVES AND THE CORRESPONDING MODELS

In order to evaluate the influence of the actuator components in the energy consumption, four actuator alternatives have been studied. The goal of this study is to

evaluate the effect of friction and actuator inertia in the energy consumption.

In all cases the mechanical power is to be provided by a DC motor. The main reason for this choice is that it is easily controllable and therefore quite convenient for the actuation of a walking robot. The electromechanical power conversion of the motor is modelled using the information and parameters provided by the manufacturer [5]. Main variables involved in this power conversion are represented in Fig. 5.

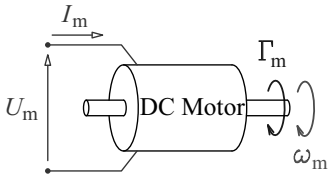

Fig. 5. Main variables in the DC motor

A mechanical reducer is needed to fit joint velocity and demanded torque to DC motor performance. The transmission ratio in all the actuator alternatives is 400:1.

Two of the actuator alternatives include ideal components. These unrealistic alternatives will be useful to compare them to the realistic ones and to show the influence of the actuator characteristics on the energy consumption.

The other two ones correspond to realistic actuator designs, the first with a reversible transmission and the second with an irreversible one.

A. Alternative 1: Ideal actuator

1) Description

This hypothetical actuator would consist of a DC motor as a power conversion unit, but with neither inertia nor friction between moving parts, and an ideal transmission, also without inertia nor friction.

2) Transmission model

The main variables involved in the ideal actuator model are represented in Fig. 6. The required motor torque can be calculated from the mechanical power balance of the ideal transmission (see Eq. 1).

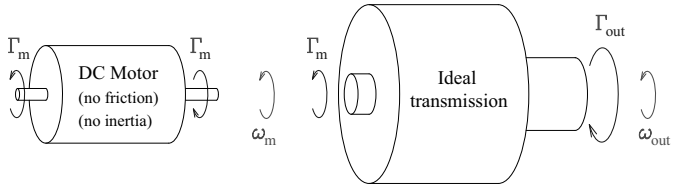

Fig. 6. Main variables in the ideal actuator.

$$\Gamma_m \cdot \omega_m = \Gamma_{out} \cdot \omega_{out} \quad (1)$$

B. Alternative 2: Actuator with ideal transmission

1) Description

This actuator consists of a DC motor, this time including rotor inertia and friction, and an ideal transmission with no friction nor inertia.

2) Transmission model

The main variables involved in the mechanical model of this actuator are shown in Fig. 7. The transmitted torque between motor and ideal transmission, Γ_{mt}, can be calculated from the mechanical power balance of the ideal transmission (see Eq. 2).

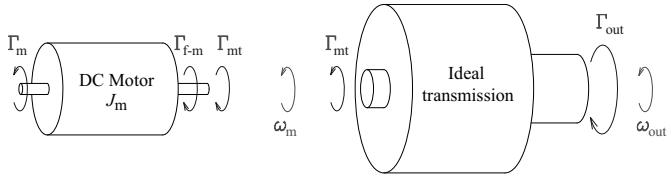

Fig. 7. Main variables in the actuator with ideal transmission.

$$\Gamma_{mt} \cdot \omega_m = \Gamma_{out} \cdot \omega_{out} \quad (2)$$

The required motor torque can be calculated from the mechanical power balance at the rotor (see Eq. 3), and the estimated friction torque on the rotor is calculated according to Eq. 4, where Γ_0 and c were determined from experimental tests [6].

$$\Gamma_m \cdot \omega_m = \Gamma_{mt} \cdot \omega_m + \Gamma_{f\text{-}m} \cdot \omega_m + J_m \cdot \omega_m \cdot \dot{\omega}_m \quad (3)$$

$$\Gamma_{f-m} = \left(\Gamma_o + c \cdot |\omega_m|\right) \cdot \mathrm{sgn}(\omega_m) \quad (4)$$

C. Alternative 3: Reversible actuator

1) Description

This actuator consists of a DC motor, a timing belt transmission and a *Harmonic Drive*® reducer. Important advantages of the *HD* gear are the low weight, high transmission ratio, and high efficiency. Each joint is directly implemented by an *HD* assembly (see the CAD model in Fig. 8).

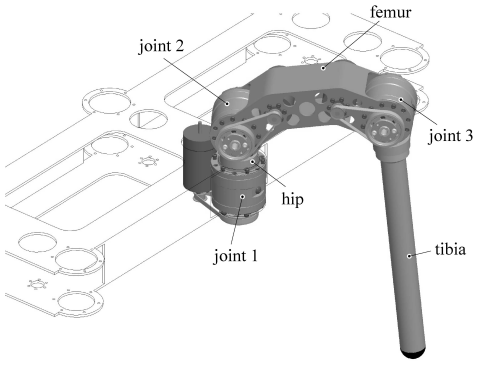

Fig. 8. Reversible actuator integration in the middle-right leg.

2) Transmission model

The main variables involved in the mechanical model of this actuator are shown in Fig. 9.

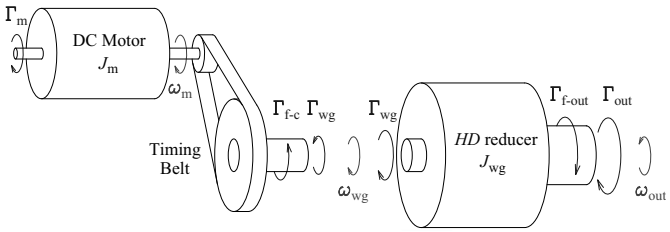

Fig. 9. Main variables in the reversible actuator.

In the *HD* reducer model, the friction torque on the output shaft, $\Gamma_{\text{f-out}}$, characterizes all the frictional effects in the reducer. This friction torque is estimated according to Eq. 5, where parameters Γ_0, μ and c were determined by experimental tests of an actuator prototype [6].

$$\Gamma_{\text{f-out}} = \left(\Gamma_{\text{o}} + \mu \cdot \Gamma_{\text{out}} + c \cdot \omega_{\text{out}}\right) \cdot \text{sgn}\left(\omega_{\text{out}}\right) \tag{5}$$

Similarly, the torque friction $\Gamma_{\text{f-c}}$ characterizes all the frictional effects in the timing belt transmission, including the friction in the rotor. This friction torque is estimated using Eq. 6, where parameters Γ_0, μ and c were determined by experimental tests of an actuator prototype [6].

$$\Gamma_{\text{f-c}} = \left(\Gamma_{\text{o}} + \mu \cdot \Gamma_{\text{wg}} + c \cdot \omega_{\text{wg}}\right) \cdot \text{sgn}\left(\omega_{\text{wg}}\right) \tag{6}$$

The transmitted torque between timing belt and *HD* reducer, Γ_{wg}, can be calculated from the mechanical power balance of the *HD* reducer (see Eq. 7).

$$\Gamma_{\text{wg}} \cdot \omega_{\text{wg}} - \Gamma_{\text{out}} \cdot \omega_{\text{out}} - \Gamma_{\text{f-out}} \cdot \omega_{\text{out}} = J_{\text{wg}} \cdot \omega_{\text{wg}} \cdot \dot{\omega}_{\text{wg}} \tag{7}$$

The required motor torque, Γ_{m}, can be calculated from the mechanical power balance of the timing belt transmission (see Eq. 8).

$$\Gamma_{\text{m}} \cdot \omega_{\text{m}} - \Gamma_{\text{wg}} \cdot \omega_{\text{wg}} - \Gamma_{\text{f-c}} \cdot \omega_{\text{wg}} = J_{\text{m}} \cdot \omega_{\text{m}} \cdot \dot{\omega}_{\text{m}} \tag{8}$$

D. Alternative 4: Irreversible actuator

1) Description

This actuator consists of a DC motor, a planetary gear and a hypoid reducer. The main characteristics of hypoid gears are high transmission ratio and the offset between input and output axes. Depending on their design, hypoids can present an irreversible behaviour, meaning that the efficiency can be relatively high when power flows from the input to the output of the gear but very low or null when the power flows on the reverse direction. Every joint is directly implemented by the hypoid gear assembly (see the CAD model in Fig. 10).

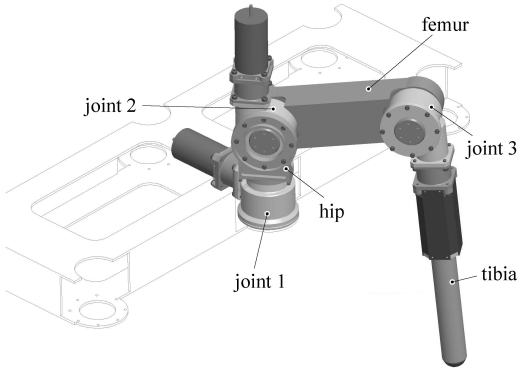

Fig. 10. Irreversible drive system for the middle-right leg.

2) Transmission model

The main variables involved in the mechanical model of the hypoid reducer are shown in Fig. 11.

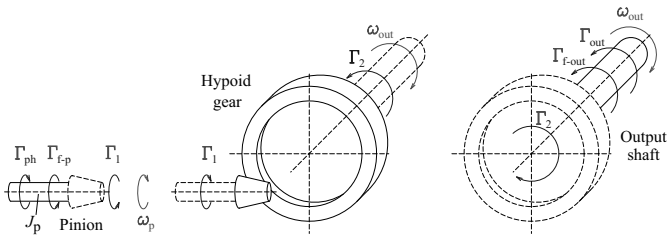

Fig. 11. Main variables in the hypoid reducer.

The torque at the output of the hypoid gear, Γ_2, can be obtained from the mechanical power balance at the output shaft (see Eq. 9). The friction torque at the output of the actuator, $\Gamma_{\text{f-out}}$, is calculated in Eq. 10, where Γ_0 and c were estimated from bearing data.

$$\Gamma_2 \cdot \omega_{\text{out}} = \Gamma_{\text{out}} \cdot \omega_{\text{out}} + \Gamma_{\text{f-out}} \cdot \omega_{\text{out}} \tag{9}$$

$$\Gamma_{\text{f-out}} = \left(\Gamma_{\text{o}} + c \cdot \left|\omega_{\text{out}}\right|\right) \cdot \text{sgn}(\omega_{\text{out}}) \tag{10}$$

The mechanical power balance at the hypoid gear is presented in Eq. 11. The resultant normal force at the teeth contact, F_{n}, is calculated according to Eq. 12, where β_2 and r_2

are parameters of the gear and μ is the friction coefficient at the teeth contact.

$$\Gamma_1 \cdot \omega_p = \Gamma_2 \cdot \omega_{out} \tag{11}$$

$$F_n = \frac{\Gamma_2}{r_2} \cdot \frac{1}{\cos\beta_2 + \mathrm{sgn}(\omega_{out})\,\mathrm{sgn}(\Gamma_2)\,\mu \sin\beta_2} \tag{12}$$

Then, the torque at the hypoid gear input, Γ_1, can be obtained from Eq. 13, where β_1 and r_1 are parameters of the pinion and μ is the friction coefficient.

$$\Gamma_1 = \left[F_n \cdot \cos\beta_1 + \mathrm{sgn}(\omega_{out})\,\mu |F_n| \sin\beta_1\right] \cdot r_1 \tag{13}$$

The transmitted torque between planetary gear and the hypoid reducer, Γ_{ph}, can be obtained from the mechanical power balance at the pinion (see Eq. 14). The estimated friction torque on the pinion is calculated according to Eq. 15, where Γ_0 and c were estimated from bearing data.

$$\Gamma_{ph} \cdot \omega_p = \Gamma_1 \cdot \omega_p + \Gamma_{f\text{-}p} \cdot \omega_p + J_p \cdot \omega_p \cdot \dot{\omega}_p \tag{14}$$

$$\Gamma_{f\text{-}p} = \left(\Gamma_o + c \cdot |\omega_p|\right) \cdot \mathrm{sgn}(\omega_p) \tag{15}$$

The main variables involved in the mechanical model of the planetary reducer are shown in Fig. 12.

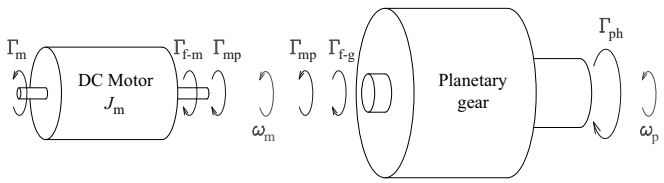

Fig. 12. Main variables in the planetary reducer.

The transmitted torque between the motor and the planetary gear, Γ_{mp}, can be obtained from the mechanical power balance at the planetary gear (see Eq. 16). According to the information provided by the manufacturer [5], the estimated friction torque on the planetary gear is considered constant and can be obtained from Eq. 17, where Γ_0 was determined from gear data.

$$\Gamma_{mp} \cdot \omega_m = \Gamma_{ph} \cdot \omega_p + \Gamma_{f\text{-}g} \cdot \omega_m \tag{16}$$

$$\Gamma_{f-g} = \Gamma_o \cdot \mathrm{sgn}(\omega_m) \tag{17}$$

Finally, the motor torque demand, Γ_m, can be obtained from the mechanical power balance at the rotor (see Eq. 18), and the estimated friction torque on the rotor, $\Gamma_{f\text{-}m}$, is calculated according to Eq. 19, where Γ_0 and c were determined from experimental tests [6].

$$\Gamma_m \cdot \omega_m = \Gamma_{mp} \cdot \omega_m + \Gamma_{f\text{-}m} \cdot \omega_m + J_m \cdot \omega_m \cdot \dot{\omega}_m \tag{18}$$

$$\Gamma_{f\text{-}m} = \left(\Gamma_o + c \cdot |\omega_m|\right) \cdot \mathrm{sgn}(\omega_m) \tag{19}$$

IV. Actuators Simulation During Robot Operation

The four actuator models presented in last section have been used to estimate their energy consumption during robot operation. The operating modes that have been analysed are the two ones considered in section II, concerning the middle-right leg of the robot. Input variables for the actuators simulation are angular velocity and demanded torque at the output of each actuator.

A. Simulation of a walking cycle

One of the results that can be obtained from the actuator simulation is the transmitted energy per walking cycle at different stages: at the output, between actuator components and from the power supply to the DC motor. The involved energy at each stage of the actuator is divided in two terms: the energy associated to the instants when the power is transmitted in the direction from the power supply to the actuator output, E_i (+), and the energy associated to the instants when the power is transmitted in the reverse direction, E_i (-). It is important to separately evaluate both terms because E_i (-) not always can be recovered to be used later in direction to the actuator output.

1) Alternative 1: Ideal actuator

In Fig. 13 a block diagram of the ideal actuator is represented. The DC motor represents the power conversion unit without including mechanical characteristics of the rotor. Total transmitted energy per cycle at the different stages is represented in Fig. 14.

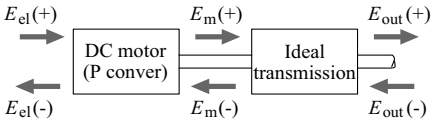

Fig. 13. Ideal actuator block diagram and energy flow through components.

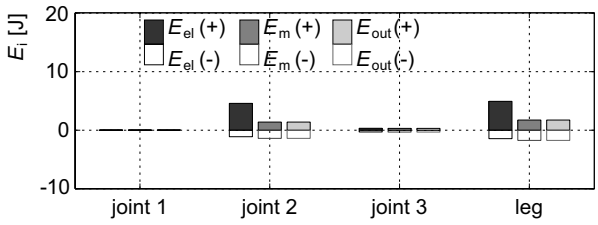

Fig. 14. Total transmitted energy per cycle through the ideal actuator components.

At each joint, the amount of energy transmitted at the output of the actuator to the joint, E_{out} (+), is the same as the energy transmitted in reverse direction, from the joint to the

actuator, E_{out} (-). The reason is that the mechanical energy of the robot is the same at the beginning and at the end of a walking cycle. So during a cycle the actuator sometimes provides mechanical power and other times absorbs it.

The energy involved at the input and at the output of the transmission is the same, since no energy is stored or dissipated in an ideal transmission.

At joint 2 the electrical energy supplied to the motor, E_{el} (+), is much higher than the mechanical energy provided by it, E_m (+), and this is because of the low efficiency of the power conversion when the motor torque is high.

2) Alternative 2: Actuator with ideal transmission

In Fig. 15 a block diagram of the actuator with an ideal transmission is represented. The DC motor is divided in two parts: one represents the power conversion system and the other represents the mechanical model of the rotor. Total transmitted energy per cycle at the different stages is represented in Fig. 16.

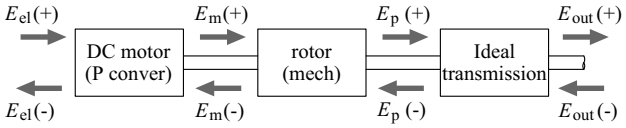

Fig. 15. Block diagram of the actuator with ideal transmission and energy flow through components.

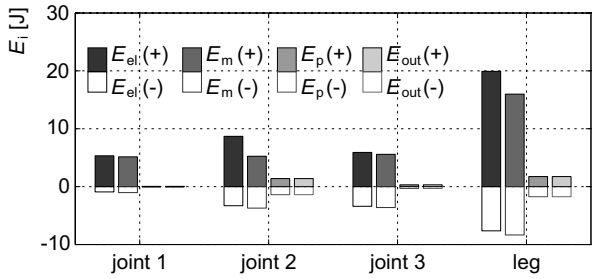

Fig. 16. Total transmitted energy per cycle through the components of the actuator with ideal transmission.

The energy involved at the input of the transmission is the same as in the case of the ideal actuator, since the model of the ideal transmission is the same.

In this case, and at all the joints, the mechanical energy to be provided by the motor conversion, E_m (+), is much higher than with the ideal actuator, because there is an important energy dissipation caused by the friction at the rotor. The fluctuation of the kinetic energy associated to the rotor rotation increases the energy dissipation in it.

3) Alternative 3: Reversible actuator

In Fig. 17 a block diagram of the reversible actuator is shown. The DC motor represents the power conversion system, and rotor inertia and friction are included in the timing belt transmission, since the rotor is the input shaft of this transmission. Total transmitted energy per cycle at the different stages is represented in Fig. 18.

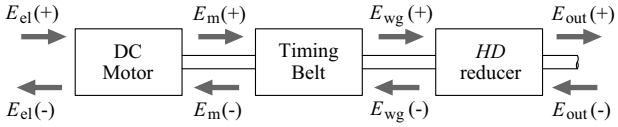

Fig. 17. Reversible actuator block diagram and energy flow through components.

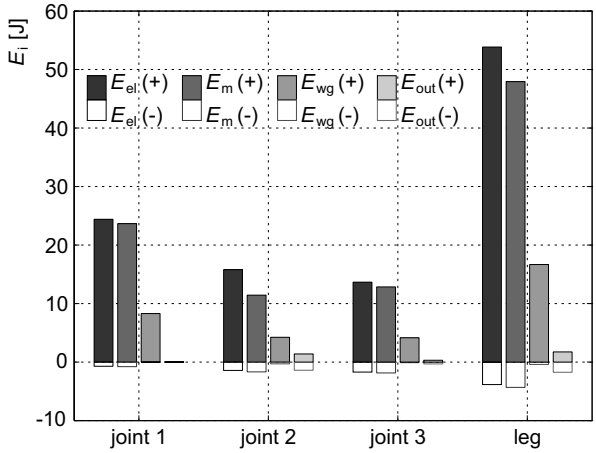

Fig. 18. Total transmitted energy per cycle through the reversible actuator components.

Although the maximum efficiency of the *HD* reducer is very high, the variable working conditions during a cycle implies an important energy dissipation caused by friction and fluctuation of its rotational kinetic energy. As a result, the mechanical energy transmitted from the timing belt to the *HD* reducer, E_{wg} (+), is much higher than the one transmitted from it to the joint, E_{out} (+).

The same phenomena occurs in the timing belt transmission, then E_m (+), is much higher than E_{wg} (+).

4) Alternative 4: Irreversible actuator

In Fig. 19 a block diagram of the reversible actuator is shown. The DC motor represents the power conversion system, and rotor inertia and friction are included in the planetary reducer, since the rotor is the input shaft of this transmission. Total transmitted energy per cycle at the different stages is represented in Fig. 20.

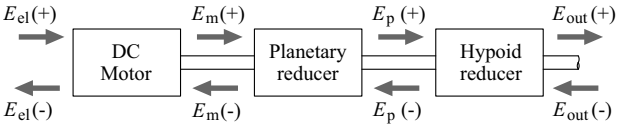

Fig. 19. Irreversible actuator block diagram and energy flow through components.

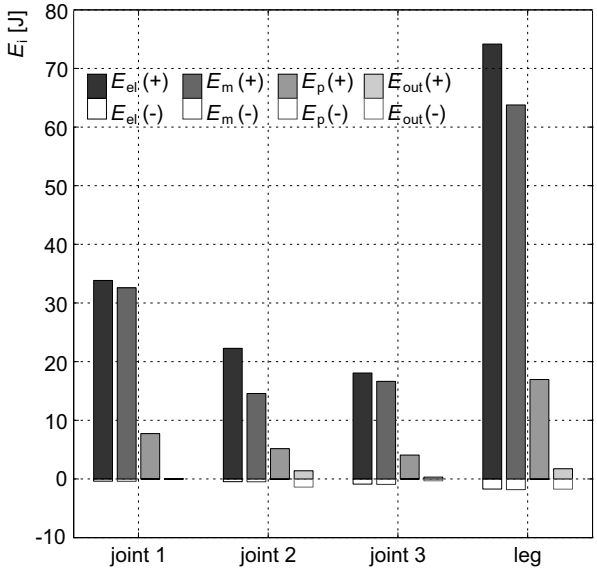

Fig. 20. Total transmitted energy per cycle through the irreversible actuator components.

The efficiency of the transmission formed by the planetary and hypoid reducers is lower than the one formed by the timing belt and the *HD* reducer. As a result the energy dissipated by friction in this case is higher than in the case of the reversible actuator and so is the mechanical energy to be provided by the motor, E_m (+).

B. Simulation of standing still situation

At joint 1 the required torque at the actuator output, Γ_{out}, is zero, so motor torque is zero no matter the actuator alternative, and therefore the electrical power consumption is null. So, in this section simulation results are presented only for joints 2 and 3.

For all the actuator alternatives, the presented results are the needed torque at the actuator output to keep the joint fixed, $\Gamma_{out,}$ the demanded motor torque, Γ_m, and the required electrical supply of the motor, U_m, I_m and P_{el}.

1) Alternative 1: Ideal actuator

Simulation results for the ideal actuator are shown in Table IV. Since there is no friction effect in the actuator, it is necessary to supply motor torque to avoid motion, even in joint 3 where Γ_{out} is rather low.

TABLE IV

SIMULATION RESULTS WHEN STANDING STILL: IDEAL ACTUATOR

	Joint 2	Joint 3
Γ_{out} [Nm]	-30,71	1,46
Γ_m [Nm]	$-76{,}8\cdot10^{-3}$	$3{,}65\cdot10^{-3}$
I_m [A]	-2,54	0,121
U_m [V]	-0,803	0,038
P_{el} [W]	2,04	0,005

At joint 2, the electrical power consumption is quite significant. The energy consumption of the whole leg during three seconds, the same duration of the studied walking cycle, is now 6,14 J.

2) Alternative 2: Actuator with ideal transmission

Simulation results for the actuator with ideal transmission are shown in Table V. In this case, the friction at the rotor implies a reduction of the required motor torque to keep fixed the joint. Then, the electrical power consumption at joint 2 is lower than in the case of the ideal actuator and becomes null at joint 3. In this case, the energy consumption of the whole leg during three seconds is 5,58 J.

TABLE V

SIMULATION RESULTS WHEN STANDING STILL: ACTUATOR WITH IDEAL TRANSMISSION

	Joint 2	Joint 3
Γ_{out} [Nm]	-30,71	1,46
Γ_m [Nm]	$-73{,}20\cdot10^{-3}$	$3\cdot10^{-5}$
I_m [A]	-2,42	0
U_m [V]	-0,766	0
P_{el} [W]	1,86	0

3) Alternative 3: Reversible actuator

Simulation results for the reversible actuator are shown in Table VI. In this case there are important friction effects at the *HD* reducer and at the timing belt transmission. The result is a lower motor torque demand at joint 2, leading to a lower electrical power consumption. At joint 3 the motor torque demand becomes negligible, so the electrical power consumption is null. Total energy consumption of the whole leg during three seconds is 2,60 J.

TABLE VI

SIMULATION RESULTS WHEN STANDING STILL: REVERSIBLE ACTUATOR

	Joint 2	Joint 3
Γ_{out} [Nm]	-30,71	1,46
Γ_m [Nm]	$-49{,}98\cdot10^{-3}$	0
I_m [A]	-1,66	0
U_m [V]	-0,523	0
P_{el} [W]	0,866	0

4) Alternative 4: Irreversible actuator

Due to transmission friction, motor torque demand when standing still becomes null at all the joints, therefore there is no electrical power consumption.

V. CONCLUSIONS

Mechanical requirements for the actuation of a hexapod leg have been determined, in two different operating modes: walking on a horizontal ground and standing still. Four

actuator alternatives have been defined. Rotational inertia and friction at every component have been modelled from experimental studies and manufacturers data. The resulting models have been used to simulate the actuator operation while walking and while standing still.

During walking operation, the more ideal are the actuator components the lower is the energy consumption. In the ideal actuator, the only effect that increases the energy consumption is the power loss of the electromechanical power conversion at the DC motor. In the case of the second alternative, due to kinetic energy fluctuation caused by rotational inertia and friction, energy consumption is 4 times higher.

When simulating the realistic actuators, kinetic energy fluctuation and friction of the transmission components provoke an important increase of energy loses. Then energy consumption of the reversible actuator is more than 10 times higher than the one of the ideal actuator, while the ratio is almost 15 times for the irreversible one.

While the robot is standing still, the more important are the friction effects the lower is the power consumption, and it is zero when using the irreversible actuator.

Then, before selecting the actuator alternative, and in order to minimize the energy consumption of the robot, designers should evaluate the fraction of time that it is supposed to run in each possible operating mode. The energy consumption of the left and right middle legs during one minute is represented in Fig. 21, depending on the fraction of time when the robot is standing still. The energy consumption using reversible actuators will be lower, unless the fraction of the time standing still is over 94%.

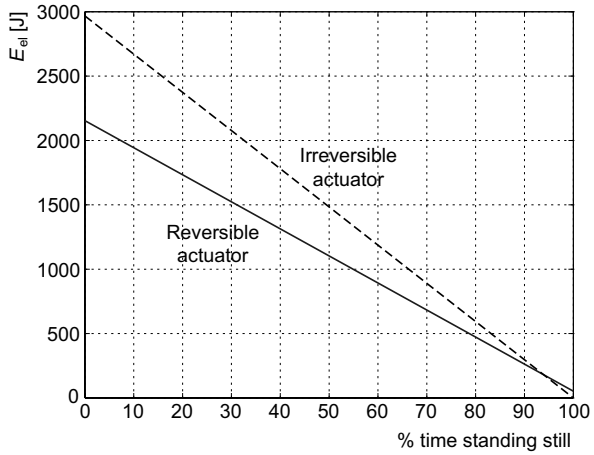

Fig. 21. Energy consumption of the middle legs during a minute.

ACKNOWLEDGEMENTS

This work has been partially supported by MCyT and FEDER funds under the project DPI2003-05193-C02-01 of the Plan Nacional de I+D+I.

REFERENCES

[1] K. Yoneda, *Design of non-bio-mimetic walker with fewer actuators*, Proc. of the 4th Int. Conf. on Climbing and Walking Robots, 2001, pp. 115-126.

[2] J. Roca, M. Nogués, S. Cardona, *Design, dynamic simulation and experimental tests of leg mechanism and driving system for a hexapod walking robot*, Proc. of the 7th Int. Conf. on Climbing and Walking Robots, pp 295-303, 2004.

[3] D. C. Kar, *Design of statically stable walking robot: a review,* Journal of Robotic Systems 20(11), 2003, pp. 671-686.

[4] S. M. Song, K. J. Waldron, *Machines that walk: the adaptive suspension vehicle*, Ed. MIT Press, 1989.

[5] Maxon motor, *High precision drives and systems,* catalogue 2005.

[6] J. Roca, *Desenvolupament i Caracterització d'un Accionament Rotatiu per a les Potes d'un Robot Caminador. Estudi de l'Eficiència Energètica,* PhD Thesis, Universitat Politècnica de Catalunya, 2006.